NANO LETTERS

LETTER

pubs.acs.org/NanoLett

Room-Temperature Gating of Molecular Junctions Using Few-Layer Graphene Nanogap Electrodes

Ferry Prins,[*,†,§] Amelia Barreiro,[*,†,§] Justus W. Ruitenberg,[†] Johannes S. Seldenthuis,[†] Núria Aliaga-Alcalde,[‡] Lieven M. K. Vandersypen,[†] and Herre S. J. van der Zant[†]

[†]Kavli Institute of Nanoscience, Delft University of Technology, Lorentzweg 1, 2628 CJ Delft, The Netherlands

[‡]ICREA, Institució Catalana de Recerca i Estudis Avançats, Departament de Química Inorgànica, Universitat de Barcelona, Martí i Frances 1-11, 08028 Barcelona, Spain

Supporting Information

ABSTRACT: We report on a method to fabricate and measure gateable molecular junctions that are stable at room temperature. The devices are made by depositing molecules inside a few-layer graphene nanogap, formed by feedback controlled electroburning. The gaps have separations on the order of 1−2 nm as estimated from a Simmons model for tunneling. The molecular junctions display gateable $I-V$-characteristics at room temperature.

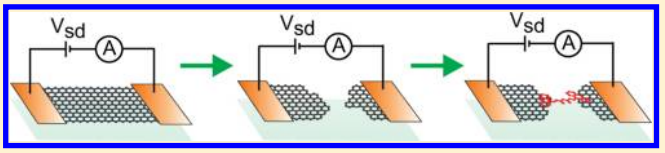

KEYWORDS: Molecular electronics, graphene, nanoelectrodes, single-electron tunneling

Molecular electronics has been the subject of extensive research over the past decade,[1,2] motivated by the appealing concept that molecules can be used as ultimate downscaled functional units in electronic circuits performing a variety of functions, including rectifiers,[3,4] switches,[5] transistors,[6−8] or sensors.[9] To date, three-terminal experiments have mostly been carried out at low temperatures, whereas for applications room-temperature operation is desirable. Device-stability is a first requirement for this but at the same time remains one of the great challenges in this field. Gold, the preferred electrode material because of its noble character, has such high atomic mobility that at room temperature the nanoelectrodes are unstable.[10] Recently it was shown that electrodes made from the more stable Pt can be used to overcome this issue,[10,11] although gated transport at room temperature has not been demonstrated yet.

An alternative strategy for the fabrication of stable electrodes with nanometer separation is the use of (sp^2-)carbon-based materials. The covalent bond-structure gives stability up to high temperatures, far beyond room temperature. Another advantage is that it allows for a large variety of possibilities to anchor diverse molecules as compared to metallic electrodes. While with the latter thiol and amine linkage is widely used,[2] the carbon-based materials can not only be functionalized covalently through organic chemistry techniques[9] but also via $\pi-\pi$ stacking interactions of aromatic rings. A third advantage is the fact that extremely thin electrodes can be prepared, ranging from (few-layer) graphene to carbon nanotubes. Compared to the more bulky metallic electrodes, the thin carbon-based electrodes reduce the screening of an applied gate-field and therefore enhance the gate coupling.

Motivated by these advantages, carbon nanotube-based nanogap electrodes have previously been constructed by oxygen-plasma etching where the gap is defined by a PMMA mask[9,12,13] or through electrical breakdown.[14−16] To date, however, control over the gap-size below 10 nm has not been demonstrated, making it difficult to contact single molecules. Other approaches that could potentially lead to nanogap electrodes include atomic force microscopy (AFM) nanolithography of graphene,[17] anisotropic etching catalyzed by nanoparticles,[18,19] graphene nanogaps formed by mechanical stress,[20] or through electrical breakdown of graphene.[21]

Here, we report on the formation of nanometer-separated few-layer graphene electrodes using feedback-controlled electroburning. The process of electroburning is related to the chemical reaction of carbon atoms with oxygen at high temperatures, induced by Joule heating at high current densities. This technique has also been utilized to controllably remove shells of multiwalled carbon nanotubes,[22−24] to form nanogaps in single-walled carbon nanotubes (SWNTs)[14−16] and to fabricate narrow graphene constrictions and quantum dots.[25,26] An important motivation for our choice for few-layer graphene (as opposed to single layer graphene or carbon nanotubes) is that it is thin, yet its conductance largely gate-independent so that features of the contacted molecules will not be masked by the electrode's response to the gate.

We start by briefly describing our fabrication technique. Few-layer graphene flakes (between 3−18 nm thick) are deposited by mechanical exfoliation of kish graphite (Toshiba Ceramics) on degenerately doped silicon substrates coated with 280 nm of thermal silicon oxide. We use standard wafer protection tape as it leaves little adhesive residue on substrates. Cr/Au electrodes are patterned on top of selected few-layer graphene flakes by electron-beam lithography and subsequent metal evaporation, followed by a

Received: June 20, 2011
Revised: October 6, 2011
Published: October 19, 2011

lift-off in cold acetone and dicholoroethane. Figure 1a (top) shows a schematic of the few-layer graphene device used for electroburning and nanogap formation. Initial device resistances at low bias are in the order of 200 Ω to 3 kΩ.

The feedback controlled electroburning is performed in air at room temperature. The feedback control scheme is based on similar methods used for electromigration of metallic nanowires.[10,27] Typically, a voltage (V) ramp is applied to the graphite flake (1 V/s), while the current (I) is continuously recorded with a 200 μs sampling rate. The variations in the conductance ($G = I/V$) are monitored with a feedback condition set at a >10% drop in G within the past 200 mV of the ramp. Upon the occurrence of such a drop, the voltage is swept back to zero in 10 ms. Immediately after, a new sweep starts from zero voltage and the process is repeated, in this way gradually narrowing down the flake.

Figure 1b shows a typical evolution of feedback-controlled electroburning. Generally, during the first voltage ramp (red trace in Figure 1b) nonlinear $I-V$ characteristics are observed, likely due to removal of contaminants on the flake by current annealing.[28] Increasing the voltage further induces the first electroburning event, as can be seen from the downward curvature in the $I-V$ characteristic, here at $V = 4.8$ V and $I = 15$ mA. The feedback then sweeps the voltage back to 0 V and a new voltage ramp is started. As the electroburning process evolves, the conductance decreases in steps and the voltage at which the electroburning occurs decreases (see green arrow in Figure 1b). In total, we have performed electroburning on 38 samples of which 35 (92%) underwent the electroburning process down to a low-bias resistance in the range of 500 MΩ to 10 GΩ. In the other cases the feedback was not fast enough to respond, resulting in gaps with infinite resistance (>100 GΩ).

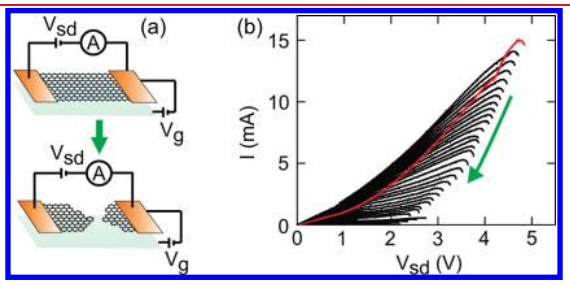

Figure 1. (a) Schematic of the feedback-controlled electroburning process, before (top) and after (bottom), the formation of nanometer sized gaps in few-layer graphite flakes. (b) Current−voltage ($I-V$) traces of the evolution (green arrow) of the feedback-controlled electroburning. The first $I-V$ trace is displayed in red.

Analyzing the cross-section of the device in Figure 1b by AFM we calculate the critical current density at which the first electroburning event occurs to be 5.3×10^7 A/cm^2. For all the devices on which we have performed the electroburning the critical current densities are comparable, between 3.8×10^7 and 7.6×10^7 A/cm^2, independent of the thickness of the flakes and similar to the current densities of 10^8 A/cm^2 at which single layer graphene breaks down.[29]

To characterize the gap geometry, we have performed AFM on several devices after electroburning, a representative example of which is shown in Figure 2. This graphite flake has a height of 12 nm, corresponding to ca. 35 layers of graphene. The image suggests that the electroburning starts from the edges in the central region of the flake, predominantly at one side. Interestingly, the height of the few-layer graphene electrodes does not change during the process of electroburning. The evolution of the thinning can be understood by considering that the electroburning is a temperature activated process, relying on the reaction of carbon atoms in the lattice with oxygen. The highest temperature in the flake as a result of Joule heating at large current densities is reached in the central region since heat is evacuated mainly to the Au-leads, while the edge-carbon atoms are the most reactive sites due to the incomplete sp^2-hybridization.[30,31] After the first carbon atoms have been removed on the site of highest reactivity, the electroburning will likely propagate from there as the current density and therefore the temperature is the highest near this point.

Because it is difficult to obtain an accurate gapsize from AFM characterization, we turn to the electrical characteristics of the nanogaps. Current−voltage characteristics between ±500 mV of 34 electro-burned samples with finite resistance were recorded at room temperature in a vacuum probe station (see Figure 3 for an example). The junctions show current−voltage curves indicative of tunneling behavior through a single barrier. The fact that we observe tunnel currents at these low biases shows that the gaps are in the order of a few nanometers. The Simmons model can be used to estimate the gap-size[32] using the gap-size, the barrier height and the asymmetry in the bias-voltage response as fit parameters (see Supporting Information for the implementation). Fits of the $I-V$-characteristics to this model yield typical gap sizes of approximately 1−2 nm.[33] The fitted barrier heights (<1 eV) are lower than one would typically expect for bulk graphite. However, low barrier heights have also been observed for nanometer-sized Au electrodes.[34]

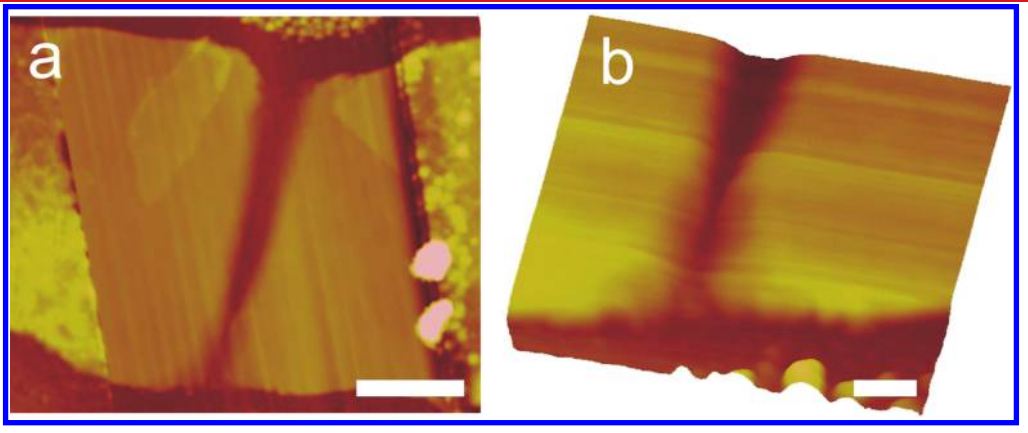

Figure 2. (a) AFM image of a typical graphite nanogap. The scale bar is 1 μm. (b) Aerial view of a zoom-in on the gap area. The scale bar is 100 nm.

dx.doi.org/10.1021/nl202065x |Nano Lett. 2011, 11, 4607–4611

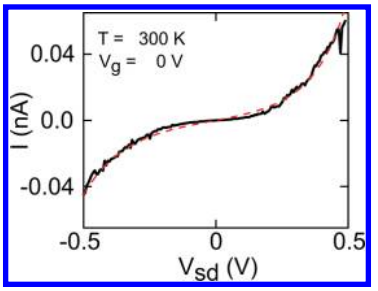

Figure 3. Representative current−voltage characteristic of a graphite nanogap (black solid line) with a fit to the Simmons model for tunneling (red dashed line). Fit parameters (accuracy of 5%): gapsize d, 2.1 nm; prefactor A, 0.34 A eV^{-2}; barrier height ϕ, 0.92 eV; asymmetry α, −0.35 (see Supporting Information for more details and the definition of the parameters).

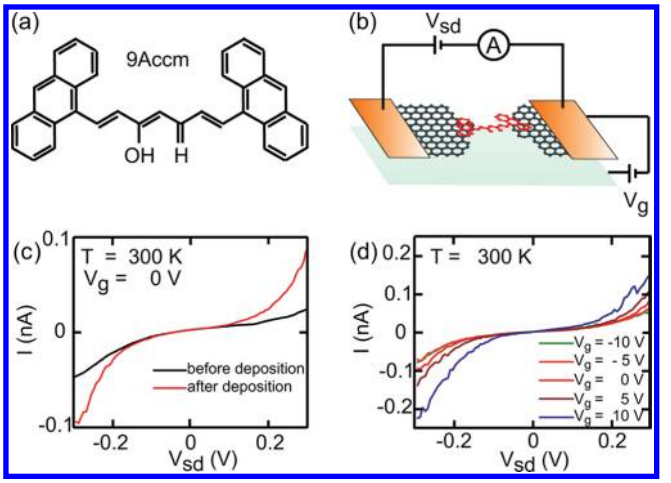

Figure 4. (a) Chemical structure of the anthracene terminated curcuminoid wires (1,7-(di-9-anthracene)-1,6-heptadiene-3,5-dione). (b) Artist's impression of a single 9Accm molecule bridging a graphene nanogap, representing the ideal transistor configuration. Note that the ambient conditions to which the devices are exposed may result in a thin layer of adsorbates such as water to be present on the surface of the few-layer graphene. (c) $I-V$-characteristics of the nanogapped electrodes before and after being bridged by the 9Accm molecules at 300 K. While the conductance at low bias superimposes with the empty gap characteristic, at higher bias a clear current increase is observed. (d) Dependence of the $I-V$ characteristics of the nanogapped electrodes bridged by 9Accm molecules on the applied back-gate voltage measured at 300 K.

Our few-layer graphene nanogap electrodes are remarkably stable and display only small variations in the tunneling characteristics after several weeks when stored in vacuum (current-levels stay within 10% variation).[35] We have also carefully measured the conductance as a function of the backgate voltage (V_g) at low temperature (10 K) at low bias voltages of typically 100 and 200 mV. Generally, for these devices the conductance does not vary within our experimentally accessible range of V_g between ±40 V.[36] The small electrode separations and long-term stability of the nanogaps, combined with the absence of gate-dependent transport across the gap imply that they can be used to contact small molecules and measure three-terminal transport.

To demonstrate this, we have deposited anthracene-functionalized curcuminoid molecules (1,7-(di-9-anthracene)-1,6-heptadiene-3,5-dione, abbreviated as 9Accm, see Figure 4a) on the nanogap devices.[37] The anthracene-groups are extended π-conjugated systems that interact strongly with the π-system of the top graphene layer, providing a strong anchor to the electrodes, while the curcuminoid wire has a high π-electron density that can mediate charge transport. We deposit the molecules by placing the devices overnight in a chloroform solution containing 0.1 mM of 9Accm. After taking the devices out of the solution they are blow-dried by a flow of N_2. AFM characterization of the deposition on a reference sample shows that a submonolayer of molecules is formed on the devices (see Supporting Information). The devices are then electrically characterized in a vacuum probe station (see Figure 4b for a schematic representation).

An important advantage of stable nanogap electrodes is that the current−voltage characteristics after deposition can be compared with the characteristics before deposition. Changes in the transport-characteristics can then be attributed to the presence of molecules in the gap. In our case, 14 out of 35 devices displayed an increase in conductance after deposition. Figure 4c shows a typical device in which such changes in the $I-V$-characteristic are observed. While the conductance at low bias superimposes with the empty gap characteristic, at higher bias a clear current increase is observed. Exposure of the devices to pure solvent (chloroform) does not show any significant changes in the electrical characteristics (see Supporting Information).

Importantly, the conductance in this device is dependent on the gate-voltage at room temperature, as illustrated in Figure 4d. Taking current−voltage characteristics at different gate voltages between −10 and 10 V, the conductance increases toward more positive gate values; that is, the blue curve in Figure 4d displays the highest currents. The gate-dependent characteristics are robust, showing only minor variations in the conductance (<10%) for periods of several weeks when stored in vacuum, and even after thermal cycling to low temperatures (10 K, see below). In total, we observed gate-modulated transport in 4 out of the 14 junctions that displayed an increase in conductance after deposition.

At low temperature (10 K), the gate-dependent transport becomes more apparent and we can moreover compare it to the empty-gap gate-dependence taken before deposition. In Figure 5a the conductance at V_{sd} = −200 mV is plotted as a function of gate voltage before and after deposition (same device as Figure 4c,d). While the conductance is gate-independent before deposition, after deposition a clear modulation of the conductance is present toward more positive values of V_g, consistent with the room temperature $I-V$-characteristics. For a full characterization, we construct conductance maps at 10 K, in which $I-V$s are taken between V_{sd} = ±300 mV while the backgate voltage is swept between ±30 V at 100 mV intervals. An example is shown in Figure 5b. In the green regions, transport is blocked due to charge quantization in the molecule, while in the red and blue regions the blockade is lifted and single electron tunneling occurs. Although the signatures may originate from a few molecules in parallel, Coulomb-blockaded transport and the single-electron tunneling nature of the transport is apparent from the conductance map.

In conclusion, we report on a new method to controllably form nanogaps in few-layer graphene with nanometer separations based on feedback controlled electroburning of few-layer graphene. Gateable transport through molecules contacted between the electrodes demonstrates the potential of room-temperature operation of molecular devices. Combined with the observed stability in time, our study shows that few-layer graphene nanogaps are an interesting alternative to metal electrodes. We further note that the fabrication technique is not limited to

dx.doi.org/10.1021/nl202065x |*Nano Lett.* 2011, 11, 4607–4611

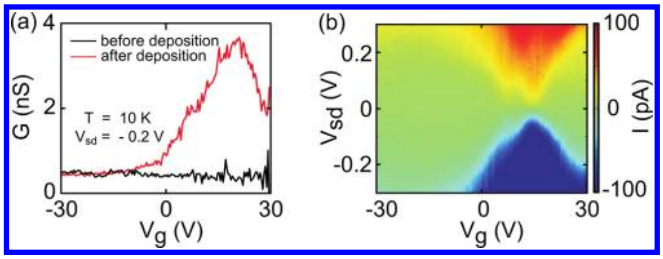

Figure 5. (a) Conductance as a function of the applied back-gate voltage of the nanogapped electrodes bridged by 9Accm molecules at 10 K. While the empty nanogap electrodes show no dependence of the applied back-gate voltage, a clear conductance modulation as a function of V_g is observed after deposition of 9Accm molecules. (b) Current map at 10 K. $I-Vs$ are taken between $V_{sd} = \pm$ 300 mV while the backgate voltage is swept between ±30 V at 100 mV intervals. In the green regions, transport is blocked due to charge quantization in the molecule, while in the red and blue regions the blockade is lifted and single-electron tunneling occurs. Although the signatures may originate from a few molecules in parallel, the single electron tunneling nature of the transport is apparent from the current map.

the use of exfoliated graphene but could also be applied to CVD-grown few-layer graphene over large areas, paving the path to more complex, integrated devices involving multiple molecular devices integrated on the same chip.

■ ASSOCIATED CONTENT

Supporting Information. Additional information and figures. This material is available free of charge via the Internet at http://pubs.acs.org.

■ AUTHOR INFORMATION

Corresponding Author

*E-mail: (F.P.) f.prins@tudelft.nl; (A.B.) a.barreiromegino@tudelft.nl.

Author Contributions

§These authors contributed equally.

■ ACKNOWLEDGMENT

We gratefully acknowledge discussions with J. M. Thijssen and we thank A. M. Goossens for experimental help. Financial support was obtained from the Dutch Foundation for Fundamental Research on Matter (FOM), and from the EU FP7 program under the Grant Agreement "ELFOS." N.A.A. thanks the Ministerio de Educación y Ciencia (CTQ2009-06959/BQU) and ICREA (Institució Catalana de Recerca i Estudis Avançats) for the financial support.

■ REFERENCES

(1) Moth-Poulsen, K.; Bjornholm, T. *Nat. Nanotechnol.* **2009**, *4*, 551–556.
(2) Song, H.; Reed, M.; Lee, T. *Adv. Mater.* **2011**, *23*, 1583.
(3) Aviram, A.; Ratner, M. A. *Chem. Phys. Lett.* **1974**, *29*, 277–283.
(4) Metzger, R. M.; Chen, B.; Hopfner, U.; Lakshmikantham, M. V.; Vuillaume, D.; Kawai, T.; Wu, X. L.; Tachibana, H.; Hughes, T. V.; Sakurai, H.; Baldwin, J. W.; Hosch, C.; Cava, M. P.; Brehmer, L.; Ashwell, G. J. *J. Am. Chem. Soc.* **1997**, *119*, 10455–10466.
(5) Blum, A. S.; Kushmerick, J. G.; Long, D. P.; Patterson, C. H.; Yang, J. C.; Henderson, J. C.; Yao, Y. X.; Tour, J. M.; Shashidhar, R.; Ratna, B. R. *Nat. Mater.* **2005**, *4*, 167–172.
(6) Park, H.; Park, J.; Lim, A. K. L.; Anderson, E. H.; Alivisatos, A. P.; McEuen, P. L. *Nature* **2000**, *407*, 57–60.
(7) Kubatkin, S.; Danilov, A.; Hjort, M.; Cornil, J.; Bredas, J. L.; Stuhr-Hansen, N.; Hedegard, P.; Bjornholm, T. *Nature* **2003**, *425*, 698–701.
(8) Yu, L. H.; Keane, Z. K.; Ciszek, J. W.; Cheng, L.; Stewart, M. P.; Tour, J. M.; Natelson, D. *Phys. Rev. Lett.* **2004**, *93*, 266802.
(9) Guo, X. F.; et al. *Science* **2006**, *311*, 356–359.
(10) Prins, F.; Hayashi, T.; van Steenwijk, B. J. A. D.; Gao, B.; Osorio, E. A.; Muraki, K.; van der Zant, H. S. J. *Appl. Phys. Lett.* **2009**, *94*, 123108.
(11) Prins, F.; Shaikh, A. J.; van Esch, J. H.; Eelkema, R.; van der Zant, H. S. J. *Phys. Chem. Chem. Phys.* **2011**, *13*, 14297.
(12) Guo, X. F.; Myers, M.; Xiao, S. X.; Lefenfeld, M.; Steiner, R.; Tulevski, G. S.; Tang, J. Y.; Baumert, J.; Leibfarth, F.; Yardley, J. T.; Steigerwald, M. L.; Kim, P.; Nuckolls, C. *Proc. Natl. Acad. Sci. U.S.A.* **2006**, *103*, 11452–11456.
(13) Whalley, A. C.; Steigerwald, M. L.; Guo, X.; Nuckolls, C. *J. Am. Chem. Soc.* **2007**, *129*, 12590.
(14) Qi, P. F.; Javey, A.; Rolandi, M.; Wang, Q.; Yenilmez, E.; Dai, H. J. *J. Am. Chem. Soc.* **2004**, *126*, 11774–11775.
(15) Wei, D. C.; Liu, Y. Q.; Cao, L. C.; Wang, Y.; Zhang, H. L.; Yu, G. *Nano Lett.* **2008**, *8*, 1625–1630.
(16) Marquardt, C. W.; Grunder, S.; Blaszczyk, A.; Dehm, S.; Hennrich, F.; von Lohneysen, H.; Mayor, M.; Krupke, R. *Nat. Nanotechnol.* **2010**, *5*, 863–867.
(17) He, Y. D.; Dong, H. L.; Li, T.; Wang, C. L.; Shao, W.; Zhang, Y. J.; Jiang, L.; Hu, W. P. *Appl. Phys. Lett.* **2010**, *97*, 133301.
(18) Campos, L. C.; Manfrinato, V. R.; Sanchez-Yamagishi, J. D.; Kong, J.; Jarillo-Herrero, P. *Nano Lett.* **2009**, *9*, 2600–2604.
(19) Schaffel, F.; Warner, J. H.; Bachmatiuk, A.; Rellinghaus, B.; Buchner, B.; Schultz, L.; Rummeli, M. H. *Nano Res.* **2009**, *2*, 695–705.
(20) Wang, H. M.; Zheng, Z.; Wang, Y. Y.; Qiu, J. J.; Guo, Z. B.; Shen, Z. X.; Yu, T. *Appl. Phys. Lett.* **2010**, *96*, 023106.
(21) Standley, B.; Bao, W. Z.; Zhang, H.; Bruck, J.; Lau, C. N.; Bockrath, M. *Nano Lett.* **2008**, *8*, 3345–3349.
(22) Collins, P. C.; Arnold, M. S.; Avouris, P. *Science* **2001**, *292*, 706–709.
(23) Collins, P. G.; Hersam, M.; Arnold, M.; Martel, R.; Avouris, P. *Phys. Rev. Lett.* **2001**, *86*, 3128–3131.
(24) Barreiro, A.; Rurali, R.; Hernandez, E. R.; Moser, J.; Pichler, T.; Forro, L.; Bachtold, A. *Science* **2008**, *320*, 775–778.
(25) Moser, J.; Bachtold, A. *Appl. Phys. Lett.* **2009**, *95*, 173506.
(26) Shi, S. F.; Xu, X. D.; Ralph, D. C.; McEuen, P. L. *Nano Lett.* **2011**, *11*, 1814–1818.
(27) Strachan, D. R.; Smith, D. E.; Johnston, D. E.; Park, T. H.; Therien, M. J.; Bonnell, D. A.; Johnson, A. T. *Appl. Phys. Lett.* **2005**, *86*, 043109.
(28) Moser, J.; Barreiro, A.; Bachtold, A. *Appl. Phys. Lett.* **2007**, *91*, 163513.
(29) Barreiro, A.; Lazzeri, M.; Moser, J.; Mauri, F.; Bachtold, A. *Phys. Rev. Lett.* **2009**, *103*, 076601.
(30) Warner, J. H.; Rummeli, M. H.; Ge, L.; Gemming, T.; Montanari, B.; Harrison, N. M.; Buchner, B.; Briggs, G. A. D. *Nat. Nanotechnol.* **2009**, *4*, 500–504.
(31) Jin, C. H.; Lan, H. P.; Peng, L. M.; Suenaga, K.; Iijima, S. *Phys. Rev. Lett.* **2009**, *102*, 205501.
(32) Simmons, J. G. *J. Appl. Phys.* **1963**, *34*, 1793.
(33) Note that the gap sizes appear to be larger than 1−2 nm in the AFM characterization (see Figure 2). Likely, the edges of the gaps are not completely vertical and narrow down closer to the substrate, suggesting more closely spaced layers to be located closer to the SiO_2.
(34) Mangin, A.; Anthore, A.; Della Rocca, M. L.; Boulat, E.; Lafarge, P. *Phys. Rev. B* **2009**, *80*, 235432.
(35) Once the gaps are successfully formed, it is important to avoid high bias voltages (>1.5 V) to prevent that the device switches back to a high conductance state, as described in ref 21.

(36) Occasionally we find a dependence of G on V_g, indicating that the sample is not fully electroburned and there still is a connection between the source and drain electrodes. The connection can be removed by performing an additional electroburning step, after which also for these devices we obtain few-layer graphene nanogap electrodes that do not show a response to the applied gate voltage.

(37) Aliaga-Alcalde, N.; Marques-Gallego, P.; Kraaijkamp, M.; Herranz-Lancho, C.; den Dulk, H.; Gorner, H.; Roubeau, O.; Teat, S. J.; Weyhermuller, T.; Reedijk, J. *Inorg. Chem.* **2010**, *49*, 9655–9663.